sustainability

MDPI

Article

Lab Investigation Using a Box Model and Image Analysis of a Contaminant Back-Diffusion Process from Low-Permeability Layers

Paolo Viotti [1,*], Antonella Luciano [2], Giuseppe Mancini [3] and Fabio Tatti [4]

[1] Department of Civil, Building and Environmental Engineering (DICEA), Sapienza University of Rome, Via Eudossiana 18, 00184 Rome, Italy
[2] Italian National Agency for New Technologies Energy and Sustainable Economic Development (ENEA), RC Casaccia, 00123 Rome, Italy; antonella.luciano@enea.it
[3] Electric, Electronics and Computer Engineering Department, University of Catania, Viale Andrea Doria 6, 95125 Catania, Italy; giuseppe.mancini@unict.it
[4] Italian Institute for Environmental Protection and Research (ISPRA), Via Vitaliano Brancati 48, 00144 Rome, Italy; fabio.tatti@isprambiente.it
* Correspondence: paolo.viotti@uniroma1.it; Tel.: +39-0644585512

Abstract: Contaminants stored in low-permeability soils can continue to threaten the adjacent groundwater system even after the aquifer is considered remediated. The redistribution of contaminants from low-to-high-permeability aquifer zones (Back-Diffusion) can generate a long-term plume tail, commonly considered one of the main obstacles to effective groundwater remediation. In this paper, a laboratory test was performed to reproduce the redistribution process from low-permeability silt lenses ($k \approx 1 \times 10^{-7}$ m/s) to high-permeability sand aquifers ($k \approx 1 \times 10^{-3}$ m/s). The target of the experimental and numerical approach was finalized to verify what influence the shape and position of the lenses could have, with respect to the bulk flow, on the time necessary to complete the depletion of the dissolved substances present in the lenses. For this purpose, an image analysis procedure was used to estimate the diffusive flux of contaminants released by these low-permeability zones in different boundary conditions. The results obtained in the laboratory test were used to calibrate a numerical model implemented to simulate the Back-Diffusion process. Once calibrated, the numerical model was used to simulate further scenarios to evaluate the influence of the location and shape of the low-permeability lenses on the time necessary to diminish its contaminant content when subjected to a steady-state flow. The numerical model was also used to investigate the effect of different groundwater velocities on the depletion time of the process. The results show that the shape and position of the lens have an important impact on the time necessary to empty the lens, and an increase in the velocity field in the bulk medium (flow rate rising from 1.6 l/h to 2.5 l/h) does not correspond to diminishing total depletion times, as the process is mainly governed by diffusive transport inside the lens. This appears to be significant when the remediation approach relies on pumping technology. Future research will verify the behavior of the released plume in a strongly heterogeneous porous medium.

Keywords: secondary source; persistence contamination; molecular diffusion; pumping technology; remediation time

Citation: Viotti, P.; Luciano, A.; Mancini, G.; Tatti, F. Lab Investigation Using a Box Model and Image Analysis of a Contaminant Back-Diffusion Process from Low-Permeability Layers. *Sustainability* **2023**, *15*, 16950. https://doi.org/10.3390/su152416950

Academic Editors: Chengcheng Li and Xubo Gao

Received: 25 October 2023
Revised: 13 December 2023
Accepted: 14 December 2023
Published: 18 December 2023

1. Introduction

Groundwater contamination caused by human activities has brought potential threats to human health and ecosystems. The restoration of contaminated aquifers has, therefore, attracted extensive attention in the last few years [1] from several researchers and institutions. In the framework of sustainable approaches forwarded by the majority of countries, the loss of water available for drinking supply or, in general, changes in the

quality of environments that rely on groundwater for their survival and development is an important topic. Several technologies can be used to treat dissolved contaminants found in groundwater. The main issue occurs when a persistent source is encountered and groundwater remediation from the dissolved contamination does not reach a sufficient enough level to consider the site renewed [2]. Separate phases are recognized to act as long-term contaminant sources, but Dense Non-Aqueous Phase Liquid (DNAPL) or Light Non-Aqueous Phase Liquid (LNAPL) zones in aquifers are not the only cause of persistent plumes [3,4].

Long-term storage and the slow release of contaminants from low-permeability aquitards (Back-Diffusion) severely hinder aquifer remediation. Thus, contaminants from low-permeability zones are considered secondary sources of contamination after primary sources are removed or isolated [5]. Unfortunately, contaminant removal in low-permeability zones is difficult and, thus, the Back-Diffusion process represents a potential limitation to aquifer remediation [6].

Diffusion into and from low-permeability zones is recognized as a significant process in the contamination of groundwater [7,8]. This process is linked to heterogeneous aquifer composition, where dissolved substances transported from groundwater through transmissive media diffuse into low-permeability zones. This geologic situation, often encountered in many contaminated sites under remediation, can present the reverse matrix diffusion phenomenon [9–11].

Plumes from a source generate a concentration gradient between high-and-low-aquifer-permeability zones, inducing a molecular diffusive flux toward low-permeability areas (forward-diffusion). When the primary source of contamination is reduced, and the pollutant concentration in the flowing water is diminished, the concentration gradient reverses, and accumulated contaminants start to be released from the low-permeability zones into the bulk media, creating the so-called "Back-Diffusion" process [12–14].

Liu and Ball [15] discussed the problem of dissolved contaminants stored inside low-permeability zones because of Forward-Diffusion and the subsequent slow release via reverse diffusion during Pump and Treat operations. Parker et al. and Liu and Ball [13,15] demonstrated the Back-Diffusion process via field measurements after the hydraulic isolation of the primary source. Also, recent papers presented by several authors [12,16–19] have faced this problem through experimental approaches or numerical ones [20–23]. Difficulties in the application of numerical models derive from the detailed information required and probably from a lack of evidence and information that can provide at least empirical parameters or relationships to describe the macroscopic situation.

Indeed, given the difficulty of collecting field data, several studies have been performed at the lab scale [12,24,25]. Several lab experiments have been carried out using image analysis for a better description of the occurring phenomena without the use of invasive instruments [26–31]. These non-invasive techniques have also been used to study contaminant storage in low-permeability zones and to investigate subsequent Back-Diffusion processes [16,25].

Laboratory experiments have also been used to investigate different remediation technologies for contaminated low-permeability zones. Some of these studies have focused on reducing the contaminant flux released from low-permeability lenses using electrokinetic migration [32,33]; treatment with dissolved oxygen [34], sodium persulfate [35], and permanganate [36]; and testing the effect of groundwater circulation wells [24,37]. These strategies can, of course, reduce the expected remediation time, but their efficiency is unknown a priori because of the difficulty in pinpointing the contaminated low-permeability zones and the absence of detailed knowledge of the different shapes and positions of the low-permeability layers. The main objective of this study was to experimentally investigate the influence of different factors like the geometry of low-permeability zones and their positions, together with the flow regime, on solute transfer from low-permeability zones to high-permeability zones. A simulation, at a laboratory scale, of the Back-Diffusion process was carried out in a box model aquifer with two different low-permeability lenses. The

saturated lenses have different shapes (a lens is characterized by one section with a circular shape and the other by a section with a rectangular shape) and are located differently in the flow field. The rectangular lens is located on the bottom of the rebuilt aquifer, while the circular one is in the body of the high-permeability medium. The experiment aimed to evaluate the differences between a quasi-full exposure to the flow field and a limited surface in contact with the flow. A numerical model applied to a domain coincident with the experimental one was used to obtain information on the different behaviors of the system. Several authors [38,39] have remarked upon the importance of a full understanding of the principal parameters acting on such a complex process for reaching valuable consideration on the possible technologies needed to accelerate the groundwater remediation process. A complete understanding of the involved processes is crucial because in this situation; several technologies commonly used for the remediation of contaminated aquifers fail, mainly because of the high costs required to completely restore the initial conditions of aquifers. Furthermore, many of these technologies require high energy consumption, causing high impacts, which are not suitable for a "sustainable approach" to groundwater remediation, as generally requested in the latest guidelines indicated by several countries worldwide. This study has the main objective of providing evidence via the visualization of the process and the involved aspects, trying to provide new and visible information to be used in cases of remediation technology choices.

2. Materials and Methods

2.1. Experimental Set-Up

A laboratory test was performed to investigate the influence of the shape and position of lenses on the Back-Diffusion phenomenon. The test was carried out using the experimental setup described in [16]. A Plexiglas tank with dimensions of 68 cm (horizontal length) × 40 cm (height) × 7 cm (depth) was used. The tank was divided into two parts: the first chamber was necessary to control the water level, limiting, at the same time, the turbulence effects; the second was filled with a porous medium. The two resulting chambers were connected by a punched plate to enable water flow. At the end of the tank, a valve was inserted for the management of the hydraulic gradient, which controlled the flow. To prevent sand escape, a gravel layer was located before the outlet. Two peristaltic pumps connected to the first chamber and to the tap outlet were used to maintain a constant flow rate during the experiment. A UV lamp (to excite the tracer used) was positioned in front of the box, together with a 3CCD camera used to collect images (Figure 1a).

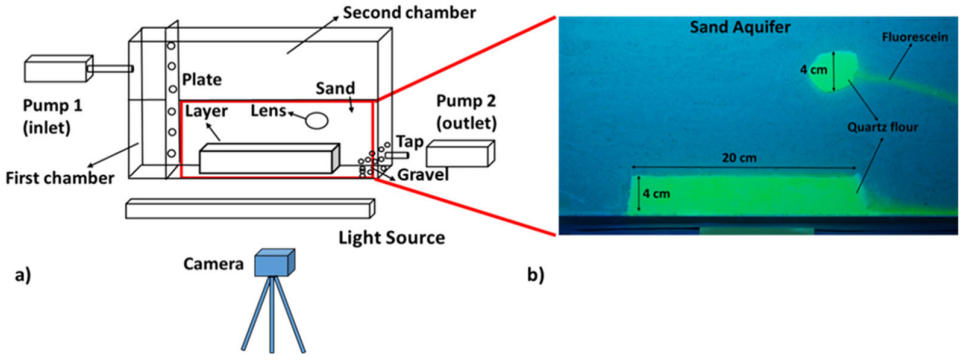

Figure 1. The experimental set-up (**a**) and the model of the reconstructed aquifer (**b**).

The aquifer model was then reconstructed inside the second chamber. The aquifer mainly consists of a high-permeability layer with two low-permeability lenses characterized by the same grain size but with different shapes (Figure 1b). The high-permeability zone of the aquifer was composed of sand and two low-permeability lenses made of quartz flour. The particle size and porosity of each material used to reproduce the aquifer were defined by laboratory measurements described by Tatti et al. [16]. The hydraulic conductivity

values of the sand and lenses were estimated using Hazen and Kozeny equations, with values reported in Table 1.

Table 1. The characteristics of the materials used to reproduce the aquifer.

	Materials	γs (kg/dm^3)	D_{50} (µm)	D_{10} (µm)	Porosity	Hydraulic Conductivity (m/s)
Sand	Quartz	2.65	700	430	0.40	3×10^{-3}
Lens	Quartz Flour	2.65	12	1.4	0.42	5×10^{-7}
Layer	Quartz Flour	2.65	12	1.4	0.42	5×10^{-7}

One of the low-permeability lenses is characterized by a cylindrical shape with a section that can be considered approximately described as a circular shape characterized by a diameter (D) of about 4–4.2 cm, a thickness of 7 cm, and a volume of about 95–100 cm^3. The other lens, hereafter referred to as the layer, can be described as a parallelepiped with a length (L) of around 20–22 cm, a high (H) similar to the diameter of the first lens, a thickness of 7 cm, and a volume of about 600 cm^3. Sodium fluorescein was used as a tracer to simulate a contaminant. It was chosen because it emits a light that varies from green to orange as a function of its concentration when it is excited by UV light. In this way, the tracer is clearly visible in the porous medium.

2.2. Image Analysis Set-Up and Calibration

To reproduce the Back-Diffusion phenomenon, the lenses were previously saturated with a solution containing 2 g/L of dissolved fluorescein, and then, they were placed in the sand layer. Clean water was flushed inside the bulk medium. These are the typical conditions in which the Back-Diffusion process starts to be active. Water was then flushed for 5 weeks with u = 0.2 m/d. During this phase, the tracer released by the lenses generated fluorescein tails, and the Back-Diffusion process was clearly visible, as reported in Figure 2, in which it is possible to observe the tails from both the lens and the layer. For the entire duration of the test, images were acquired continuously by means of a 3CCD camera with a prefixed time interval and then stored on a computer.

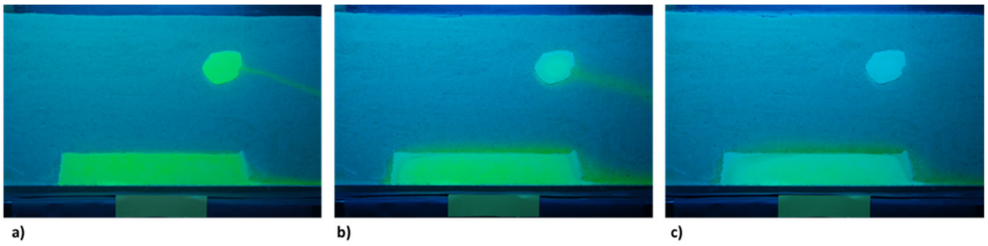

Figure 2. Images of the Back-Diffusion process collected during the first day of the test (**a**), after six days (**b,**) and five weeks (**c**) after the start of the test.

Given the importance of the definition of the times necessary for the complete restoration of an aquifer [38], the experimental set-up was used to reproduce the process of Back-Diffusion in different scenarios to evidence the influence of different macroscopic parameters on the time needed for the complete removal of the substance contained in a dissolved form inside the lenses. The lens shape's influence on the Back-Diffusion depletion time (i.e., the fluorescein mass released from the two lenses during the test) was estimated using the image analysis procedure reported in [40]. For each picture, the three color channels (RGB format) were split, and using suitable software, the spatial average intensity of the green color measured over the aquifer was defined.

A previous calibration phase allowed for the linking of the color intensity values obtained via image elaboration to the respective fluorescein concentrations. An interpolation was used to determine the analytical relationships between the fluorescein concentrations and the green light intensities. As a result, an exponential function was found, fitting the relationship between the green color intensity and the concentrations [16,19].

Equation (1) was used for the calculation of the value of the diffusive flux of fluorescein released by each lens per unit of time (J):

$$J = C \times L \times u \tag{1}$$

where L (cm) is the length of the considered section of the picture, C is the concentration obtained by means of the previous procedure, and u (cm/s) is the bulk average Darcy velocity. Multiplying the obtained value by the time interval between one image and the next, the tracer mass released by the lenses was estimated. The described image analysis procedure was validated by carrying out a mass balance of a low-permeability lens composed of quartz flour in a laboratory test reported in [40].

2.3. Numerical Model Calibration

The numerical model reported in [37] (Equations (2)–(4)) was used to study the influence of lens shape on the depletion time of the Back-Diffusion process. The model reproduces the velocity field using the classical groundwater flow equation (Equations (2) and (3)) and the distribution in time and space of the tracer in two dimensions (Equation (4)).

$$S_s \frac{\partial h}{\partial t} = \frac{\partial}{\partial x_i}\left(K_{ij}\frac{\partial h}{\partial x_j}\right) + q_s \tag{2}$$

$$u_i = -\frac{K_{ii}}{n}\frac{\partial h}{\partial x_i} \tag{3}$$

$$\frac{\partial C}{\partial t} + u_i\frac{\partial C}{\partial x_i} = \frac{\partial}{\partial x_i}\left(D_{ij}\frac{\partial C}{\partial x_j}\right) \tag{4}$$

where h is the hydraulic head (L), k_{ij} is the hydraulic conductivity tensor (LT^{-1}), S_s is the specific storage of the porous media (L^{-1}), q_s is the volumetric flux of water extracted/injected per unit of aquifer volume (T^{-1}), C is the solute concentration (ML^{-3}), u_i is the components of the velocity vector (LT^{-1}), and D_{ij} is the hydrodynamic dispersion tensor ($L^2\ T^{-1}$).

To validate the model, a laboratory test was simulated, and the experimental results were compared with the numerical ones. The calibration phase was carried out by varying the values of the hydrodynamic dispersion coefficient and the hydraulic conductivity of the porous media. Table 2 reports the final input data used in the model after the calibration phase.

Table 2. The input data used in the numerical model.

Parameter	Value	Units
Sand hydraulic conductivity	3×10^{-3}	m/s
Lens hydraulic conductivity	5×10^{-7}	m/s
Layer hydraulic conductivity	5×10^{-7}	m/s
Sand hydrodynamic dispersion	8×10^{-9}	m^2/s
Lens hydrodynamic dispersion	6×10^{-10}	m^2/s
Layer hydrodynamic dispersion	1.8×10^{-10}	m^2/s
Injection/Extraction flow rate	1.6	L/h
Initial fluorescein mass inside Lens	0.1	g
Initial fluorescein mass inside Layer	0.6	g

Inside the low permeability zones, the influence of the advective transport is practically null, and thus, the dispersivity can be considered negligible.

In the sand layer, the velocities are practically horizontal ($u \cong u_x$), the calculated mean x-component of the velocity vector result is 10^{-5} m/s, and the calibrated hydrodynamic dispersion is equal to 8×10^{-9} m^2/s. Consider the following well-known relationship:

$$D_{XX} = \alpha_L \frac{u_x^2}{u} \cong \alpha_L u_x \quad (5)$$

where α_L is the dispersivity, D_{xx} the sand hydrodynamic dispersion, and u_x the effective velocity in the x-direction, α_L is equal to 10^{-4} m, a value comparable to the sand grain size (Table 1), as expected. The transversal dispersity was assumed to be 1/10 of the longitudinal one.

The model was validated by comparing the fluorescein mass released from the lenses, determined numerically, with the one estimated via image analysis. Figures 3 and 4 show the calibration results.

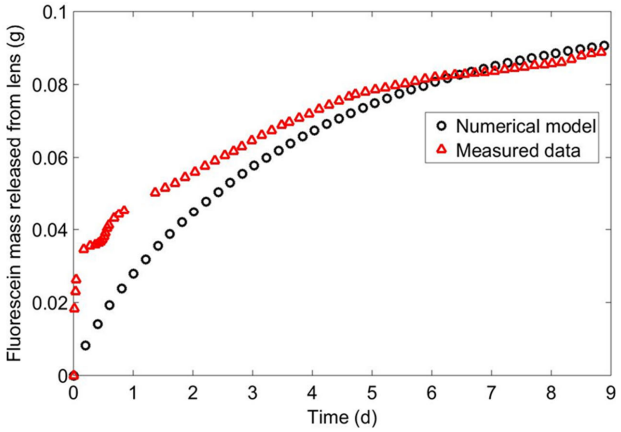

Figure 3. Model calibration phase: comparison between the experimental data and those obtained via numerical simulation for the lens.

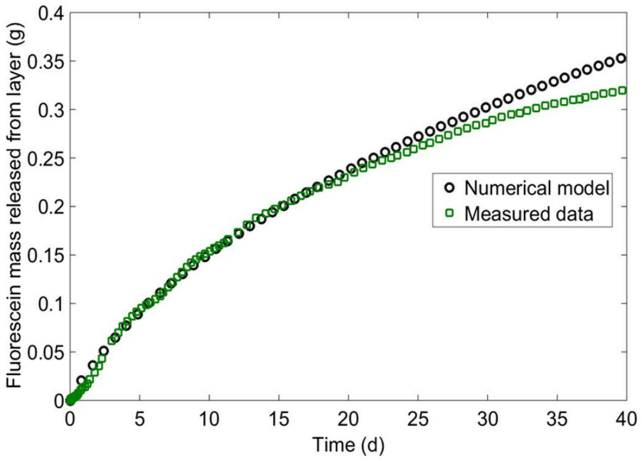

Figure 4. Model calibration phase: comparison between the experimental data and those obtained via numerical simulation for the layer.

The coefficient of efficiency, E, was adopted to evaluate the agreement between the values [25].

$$E = 1.0 - \frac{\sum_i (O_i - P_i)^2}{\sum_i (O_i - \mathrm{O})^2} \quad (6)$$

where P_i is the simulated result, O_i is the data calculated via image analysis, and O is the average of the data calculated via image analysis. Values of E closer to 1.0 indicate a better fit. The results obtained via the numerical model and image analysis were in general agreement with E = 0.88 for the lens (Figure 3) and E = 0.98 for the layer (Figure 4). The obtained values of E can be considered satisfactory in demonstrating the model's suitability in reproducing the investigated process.

3. Numerical Simulation Results

Figures 5 and 6 show, respectively, the flow field and the Back-Diffusion process simulated using the numerical model. An analysis of Figure 5 clearly shows that the flow inside the lenses is practically null, as expected, because of low permeability. Therefore, the transport inside the lenses, based on the concentration gradient in the space, depends on the molecular diffusivity. The bulk velocities are responsible for the transport outside the lenses, but inside them, the transport is totally governed by the diffusive one. The calibration shows that these elements, considered in the numerical model, respond adequately to the physical phenomena occurring at the microscale and at a larger scale. These fundamental considerations lead to the conclusion that the governing mechanism of pollutant release from the inner part of the lens occurs at the contact between the lens and the bulk medium. These elements suggest that by increasing the velocity of the bulk flow, the higher gradient existing at the interface could probably enhance the velocity of the depletion of the mass contained inside the lens.

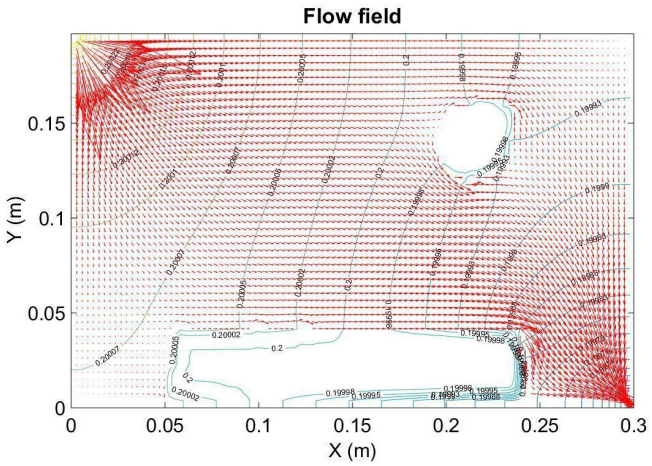

Figure 5. An image of the numerically obtained flow field in the tank.

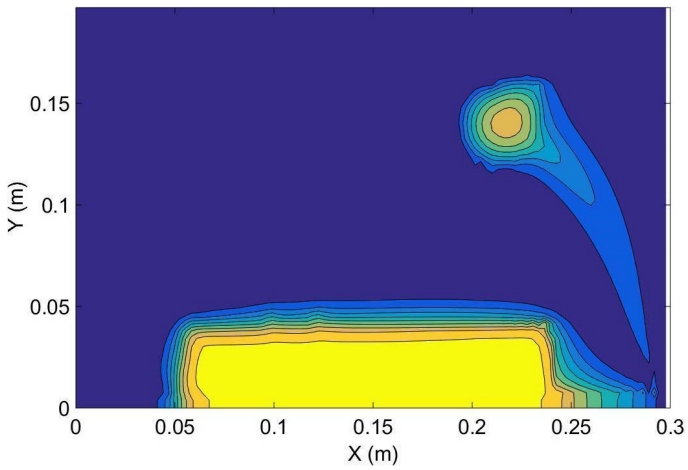

Figure 6. An image of the numerical simulation of the Back-Diffusion process. The yellow color represents the highest concentration, and blue represents the lowest.

4. Discussion

The cumulative mass of fluorescein released by the lens measured using image analysis shows a rapid increase during the first minutes of the experiment (Figure 3). This is due to several processes occurring, mainly regarding the transient phase at the beginning of the experimental test when the flow field has not yet reached steady-state conditions (Figure 7). As reported below, we can add a further element to this aspect, already evidenced in previous tests, that takes into consideration the shapes and position of the low-permeability lenses.

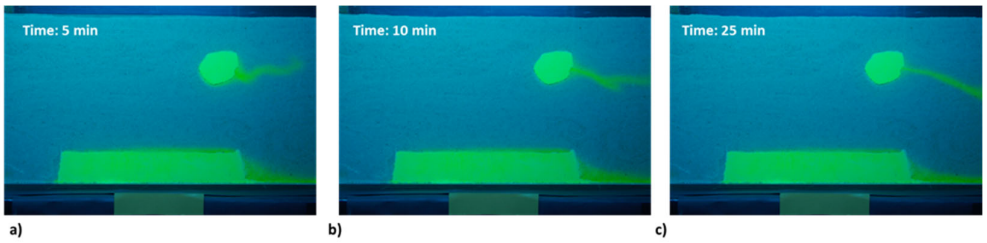

Figure 7. Images of the Back-Diffusion process taken after 5 min (**a**), 10 min (**b**) and 15 min (**c**) from the start of the experiment when the flow field was characterized by a non-steady state.

The cylindrical shape of the lens and the possible presence of zones not fully saturated inside the porous medium may have caused a pressure gradient between the lens and the sand layer. The pressure gradient was calculated using the approach reported in [40]:

$$p = \frac{3}{2}\frac{\mu\, u\, cos\, \theta}{R} \tag{7}$$

where p is the pressure, μ is the dynamic viscosity of water, u is the groundwater velocity, R is the radius of the sphere, and θ is the angle measured around the sphere from 0° at the rear point and 180° at the front point. In order to consider the non-steady state of the flow field, the pressure gradient was calculated using u values ranging from 10^{-5} m/s to 10^{-7} m/s. The Δp calculated between the front and rear points of the lens is around 7×10^{-7} Pa for $u = 10^{-5}$ m/s and 7×10^{-9} Pa for $u = 10^{-7}$ m/s. Therefore, the pressure gradient between the lens and the sand layer can be considered numerically negligible, and no consistent advective flow internal to the lenses that could be coupled to the diffusional one should be considered. Conversely, it is reasonable to assume that this slight difference in the pressure values upgradient and downgradient of the lens could have influenced the behavior, together with the above-mentioned aspects, of the beginning fluorescein tail phase, which clearly shows anomalous waves (Figure 7). The oscillating behavior has brought uncertainties in defining the mass evaluation from the image analysis. The process changes completely when the flow field has reached a steady-state condition (Figure 7c). This effect has not affected the layer located on the bottom because the difference in pressure is completely negligible thanks to its shape, and the presence of the walls of the tank limits the effects.

Another aspect that can be observed is that, in the case of the layer, during the last days of the experiment, the cumulated mass of fluorescein simulated by the model is higher than the cumulated tracer mass measured with image analysis (Figure 4). This is due to the fluorescein concentrations released by the layer after the thirtieth day, which were defined by a large error using image analysis because of their low values.

As reported previously, the lenses were reproduced using the same materials, and they were saturated with a solution containing 2 g/L of dissolved fluorescein. Thus, we can say that the unit of volume of each lens contains the same quantity of tracer (about 1 mg). In comparing the trend of cumulated fluorescein mass per unit of volume of each lens, the release of the tracer appears much slower for the layer than for the cylindrical lens (Figure 8). So, the shape of the lenses assumes great importance, as already reported in [38]. The list of important parameters mentioned in [38] continues with the physical

characteristics of both zones (low and high permeability), including hydraulic gradient; permeability; porosity; and, of course, layer geometry. However, the chemical properties and the position of the lenses with respect to the bulk flow were not considered.

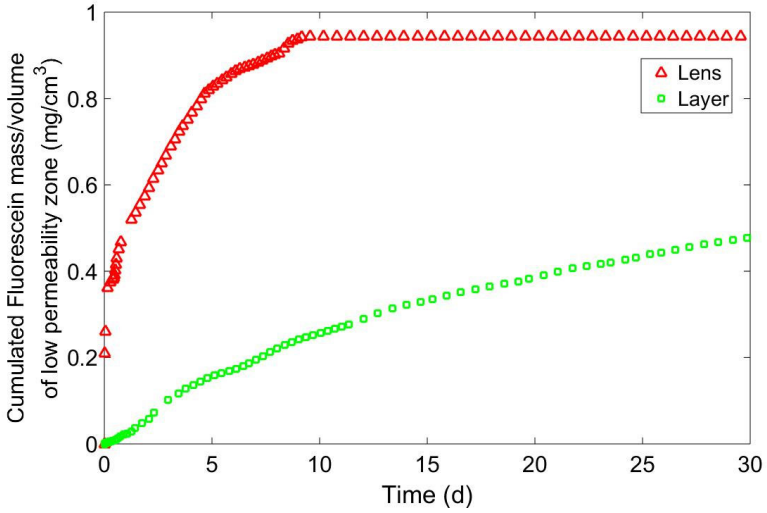

Figure 8. The trend of cumulated fluorescein mass per unit of volume measured with image analysis for each low-permeability lens.

In particular, the lens characterized by a cylindrical shape released the total fluorescein stored inside its structure during the first 10 days of the test. The layer instead continued to release the tracer even after the thirtieth day. The laboratory test was stopped after five weeks because the concentration of tracer released by the layer after the thirtieth day was too low to be estimated using the procedure based on image analysis. The slower release of fluorescein from the second lens is due to the partial exposure of the interface to the fluid motion (the bottom layer is confined to the wall of the tank), thus including the low-permeability lens position with respect to bulk flow. To confirm this hypothesis, a numerical model was used to simulate the release of fluorescein contained inside the layer in case it was positioned in the middle part of the sand layer (Figures 9 and 10).

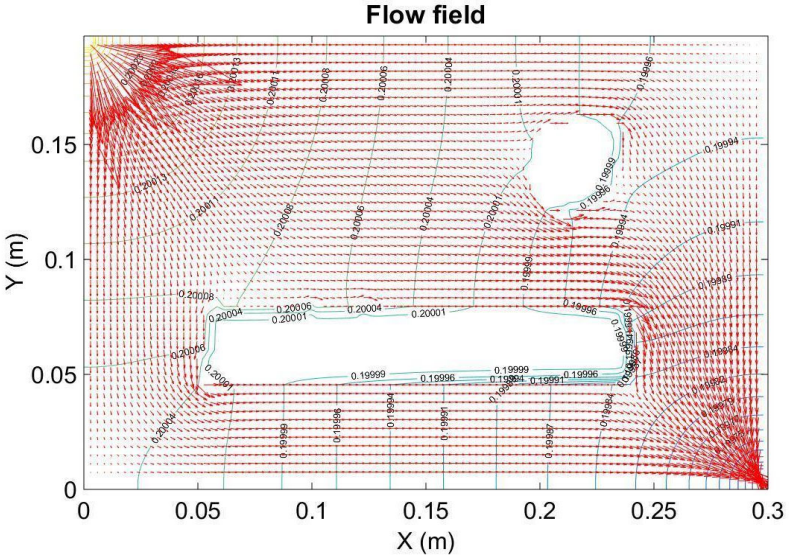

Figure 9. An image of the flow field simulated by the numerical model considering the low-permeability layer positioned in the middle part of the tank.

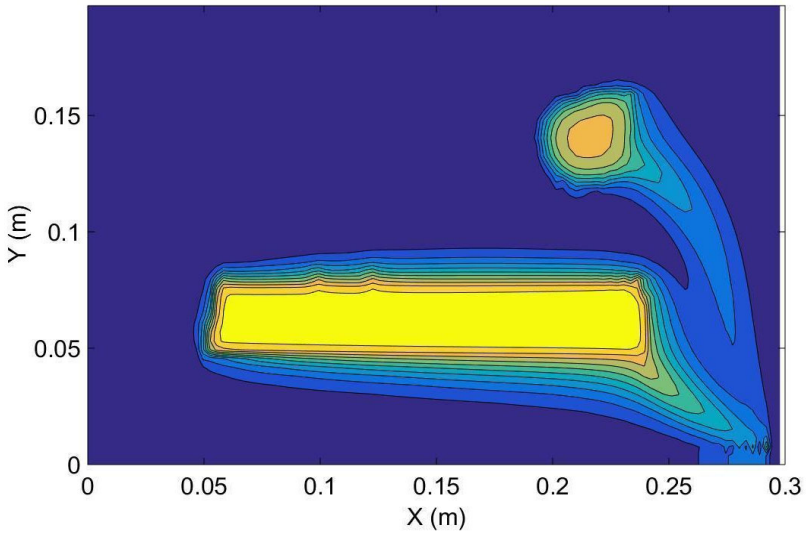

Figure 10. An image of the numerical simulation of the Back-Diffusion process considering the low-permeability layer positioned in the middle part of the tank. The yellow color represents the highest concentration, and blue represents the lowest.

For further evidence of the importance of the position of the lens in the bulk flow, a comparison was also carried out between the trends of residual fluorescein mass inside the layer located at two different points of the tank (on the bottom and in the middle part of the sand layer) (Figure 11).

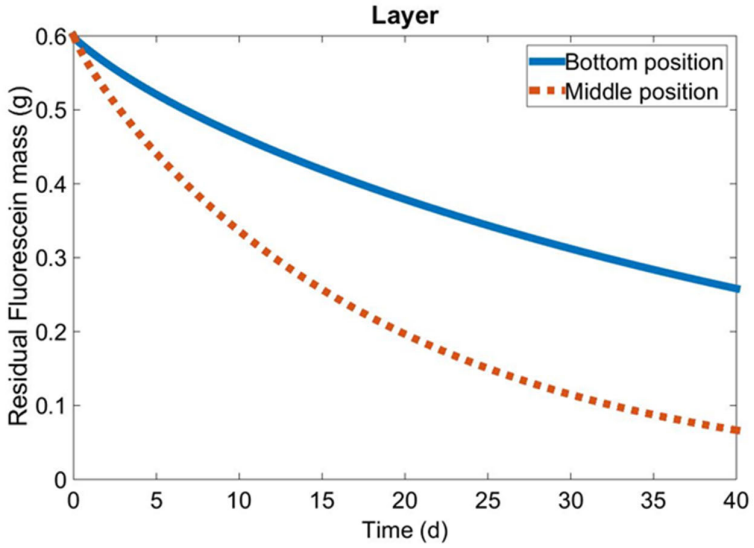

Figure 11. Image of the trend of the mass of fluorescein in the layer vs. time at two different locations in the experimental tank.

As shown in Figure 11, the layer located in the middle of the bulk flow releases fluorescein much more quickly than the layer located at the bottom of the tank, as the interface length of the layer available for fluorescein release was increased.

This result demonstrates the importance of low-permeability lens position in the domain when the Back-Diffusion process also plays an important role. For a parametric description of the importance of lens shape, the numerical model was also used to study the redistribution process of contaminants from the low-to-high-permeability zones of aquifers using a coefficient in the form of F. It is defined as the ratio between the area exposed to water flow and the volume of low-permeability lenses. It can be used to describe a lens's capacity to release contaminants stored inside its structure. The tracer is released

through the surface in contact with flowing water, and therefore, high values of F indicate great specific dispersion (per unit of volume). Coefficient F was determined for the lens characterized by a cylindrical shape and for the layer positioned in the middle part of the sand layer; respectively, the calculated values of coefficient F are 0.9 and 0.6. Comparing the depletion time of fluorescein mass in the two low-permeability zones characterized by different shapes, it is possible to note a greater release of tracer per unit of volume and, thus, a lower remediation time for the lens with respect to the layer (Figure 12). These results confirm that the depletion time of the Back-Diffusion process is strongly influenced by the shape of contaminated low-permeability zones, as reported in [38]. The importance of the shape of the low-permeability zones with regard to the contained mass depletion is confirmed in Figure 12; it is indeed possible to observe the faster depletion of the tracer content in the lens rather than in the layer located in the bulk flow. Circular lens shapes take advantage of their neutrality, which is derived from their geometry, regarding flow.

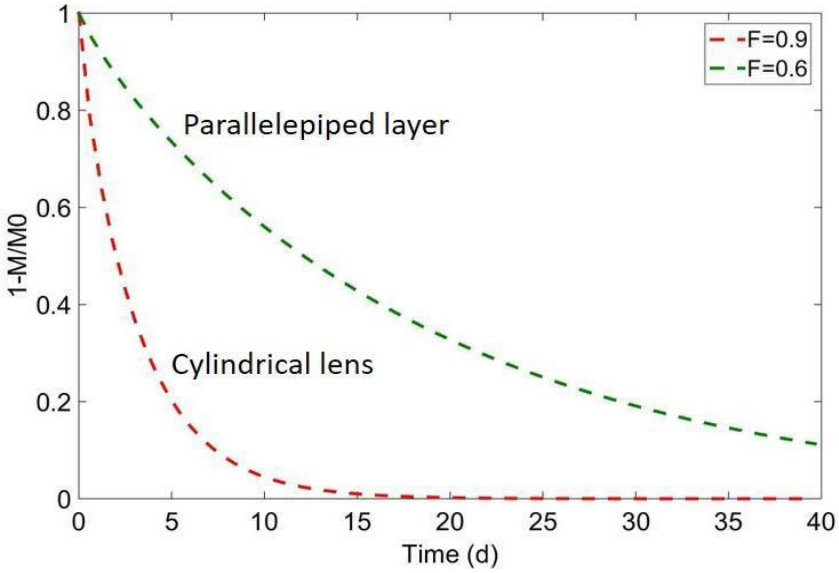

Figure 12. The trend of fluorescein mass contained in the cylindrical lens and the parallelepiped layer located in the bulk of the porous medium. The tracer mass is normalized by the total mass contained in the low-permeability zones.

In order to improve the knowledge of the management of long plume tails encountered at the field scale, a numerical model was also used to investigate the effects of the pumping technology on the contaminant redistribution process in low-permeability zones. The idea is that increasing the velocity of the bulk flow can lead to a more stable high gradient at the interface between high- and low-permeability zones. To achieve this goal, a laboratory test scheme was numerically simulated using three different injection/extraction water flow rates (Q = 0.1 L/h, Q = 0.5 L/h, and Q = 2.5 L/h), and for each lens, the trend of fluorescein mass contained in its structure was compared (Figures 13 and 14).

The results show a decrease in the tracer depletion time due to an increase in the water flow rate of both lenses, as expected. The pumping technologies develop a flow field that removes the contaminant at the interface between the high- and low-permeability zones, increasing the diffusive flux of the contaminant released by the lenses [37]. For both lenses, the reduction in tracer depletion time is lowest in the numerical simulation performed using Q = 2.5 L/h (the highest pump flow rate). Indeed, the curves of the trend of mass extracted from the lenses vs. time at 1.6 L/h can be superimposed over the one obtained at 2.5 L/h, substantially bringing them to a stop with respect to the gains obtained by increasing the pump rate. This achievement can be explained by considering how fluorescein is transported from the inner to outer areas of the low-permeability zone via diffusive flux, and this process rate is generally much lower compared with the advective transport.

The diffusive transport, even in the presence of high-concentration gradients, becomes, therefore, a limiting aspect that does not enhance the pump rate over a certain value.

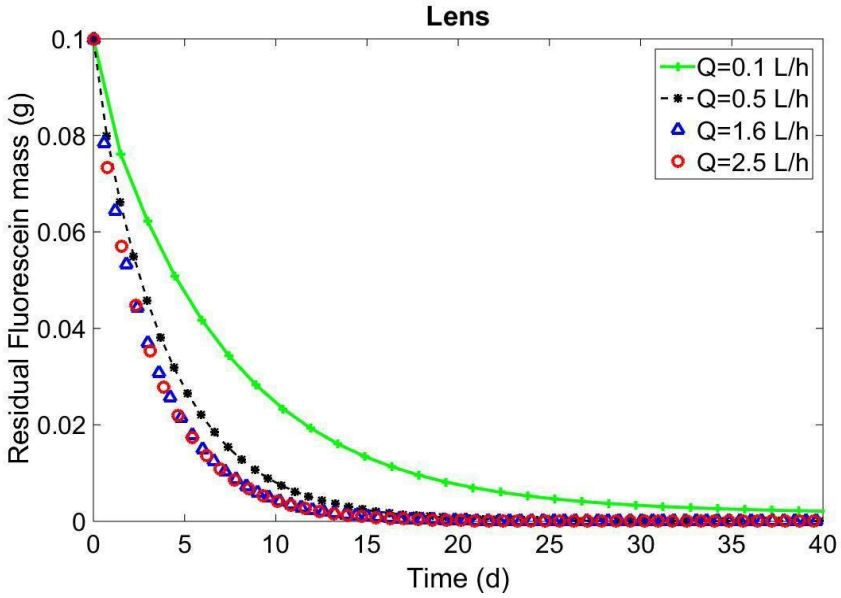

Figure 13. Image of the trend of the fluorescein mass in the lens vs. time.

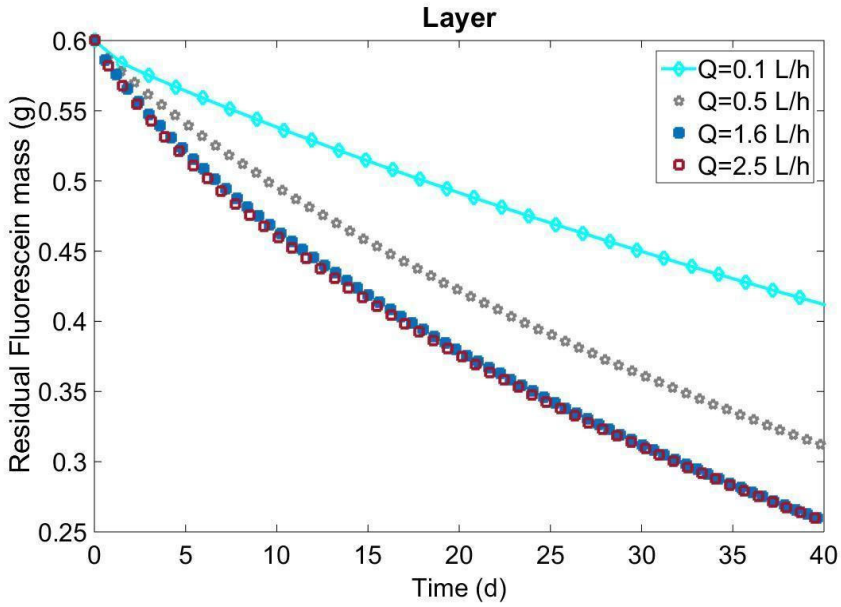

Figure 14. Image of the trend of the fluorescein mass in the layer vs. time.

The depletion time of the fluorescein mass contained inside the lenses was numerically calculated for each injection/extraction water flow rate and for each lens. The calculated depletion times for each lens were interpolated to obtain a relationship between the depletion time and the injection/extraction water flow rates. As shown in Figure 15, the data for each lens were fitted based on potential functions with good precision. The results show a reduction in Back-Diffusion depletion time correlated with an increase in the Q values, especially between Q = 0.1 L/h and Q = 0.5 L/h. The effects of the highest water flow rates investigated (Q = 1.6 L/h and Q = 2.5 L/h) appear to be negligible; therefore, the decrease in time for the complete release of the tracer confined in the lenses is practically null.

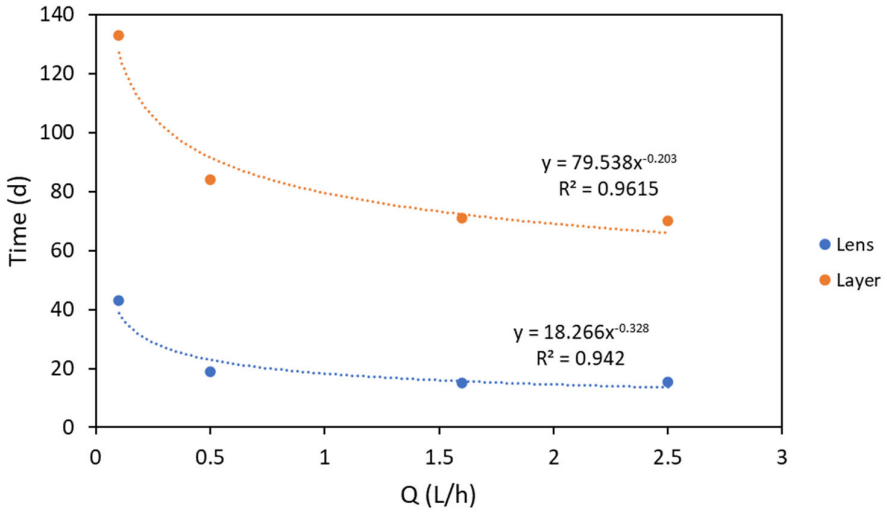

Figure 15. Trend of depletion time of the Back-Diffusion process vs. injection/extraction flow rate for the cylindrical lens and parallelepiped layer.

Considering the results of the numerical simulations performed, the application of high flow rates of injection/extraction water to accelerate the process rehabilitation of the contaminated low-permeability zones of aquifers is, therefore, not convenient if the small reduction in pollutant depletion time is compared with the high costs of the energy required for pumping and with the efforts needed to treat the extracted water, as already reported in [37,40].

5. Conclusions

The results were used to study the influence of different macroscopic variables, like the position of the two low-permeability zones, and the influence of shape and velocity in bulk medium on the "remediation time" (corresponding to the clean-up time) of each lens. The experience presented at the lab scale and the application of the numerical model have allowed for a description of the complexity of total remediation in the presence of Back-Diffusion processes. The results show that shape and location have a great impact on the "expected" remediation time. Another significant point to consider is that, when the flow rate is increased (i.e., by using a pumping system), both the efficiency and velocity of pollutant depletion reach a limit beyond which no more positive effects can be obtained. This is the stage at which the exclusively diffusive transport inside the low-permeability zone dominates the process. At that point, the time necessary for the contaminant to move from the inner part of the low-permeability zone to the boundaries, where it can interact with the bulk flow, depends only on the characteristics of the "diffusive" transport. The increase in velocity in the bulk medium, therefore, does not provide effective effects after a certain threshold, determining, therefore, the uselessness of the application of pumping technologies with high rates.

These considerations are important because the remediation technologies available and suitable for this kind of contamination are complex and expensive. A mechanical approach, for example, the use of pumping well systems, is not always able to complete the remediation process in a timeframe that can be considered acceptable from an engineering point of view.

The results obtained from the tests (both experimental and numerical) can furnish a simple suggestion on a commonly used approach to this contamination situation at a real scale; i.e., it is a good practice to test the velocity limit applied to remediation sites characterized by low-permeability lenses, at least in order to have a real expectation of the times needed to carry out the remediation. These considerations are extremely important in cases of slowly decaying or non-degradable substances.

Author Contributions: Conceptualization, P.V. and F.T.; methodology, P.V. and F.T.; software, F.T.; validation, P.V., F.T. and A.L.; formal analysis, G.M.; investigation, F.T.; resources, P.V.; data curation, P.V. and F.T.; writing—original draft preparation, P.V. and F.T.; writing—review and editing, A.L.; visualization, F.T.; supervision, P.V.; project administration, P.V.; funding acquisition, P.V. All authors have read and agreed to the published version of the manuscript.

Funding: This research received no external funding.

Institutional Review Board Statement: Not applicable.

Informed Consent Statement: Not applicable.

Data Availability Statement: Data are contained within the article.

Conflicts of Interest: The authors declare no conflict of interest.

References

1. Gao, H.; Tatomir, A.B.; Karadimitriou, N.K.; Steeb, H.; Sauter, M. Effect of Pore Space Stagnant Zones on Interphase Mass Transfer in Porous Media, for Two-Phase Flow Conditions. *Transp. Porous Media* **2023**, *146*, 639–667. [CrossRef]
2. Ding, X.H.; Feng, S.J.; Zheng, Q.T. Forward and back diffusion of reactive contaminants through multi-layer low permeability sediments. *Water Res.* **2022**, *222*, 118925. [CrossRef] [PubMed]
3. Li, Z.; Qiu, Y.; Zhao, D.; Li, J.; Li, G.; Jia, H.; Du, D.; Dang, Z.; Lu, G.; Li, X.; et al. Application of apatite particles for remediation of contaminated soil and groundwater: A review and perspectives. *Sci. Total Environ.* **2023**, *904*, 166918. [CrossRef] [PubMed]
4. Mackay, D.M.; Cherry, J.A. Groundwater contamination: Pump-and-treat remediation. *Environ. Sci. Technol.* **1989**, *23*, 630–636. [CrossRef]
5. Blue, J.; Boving, T.; Tuccillo, M.E.; Koplos, J.; Rose, J.; Brooks, M.; Burden, D. Contaminant Back Diffusion from Low-Conductivity Matrices: Case Study of Remedial Strategies. *Water* **2023**, *15*, 570. [CrossRef] [PubMed]
6. Yang, M.; Annable, M.D.; Jawitz, J.W. Field-scale forward and back diffusion through low-permeability zones. *J. Contam. Hydrol.* **2017**, *202*, 47–58. [CrossRef] [PubMed]
7. Chapman, S.W.; Parker, B.L. Plume persistence due to aquitard back diffusion following dense nonaqueous phase liquid source removal or isolation. *Water Resour. Res.* **2005**, *41*, W12411. [CrossRef]
8. Hadley, P.W.; Newell, C. The new potential for understanding groundwater contaminant transport. *Ground Water* **2014**, *52*, 174–186. [CrossRef]
9. Wilson, J.L. *Removal of Aqueous Phase Dissolved Contamination: Non-Chemically Enhanced Pump-and-Treat in Subsurface Restoration*; Ward, C.H., Cherry, J.A., Scalf, M.R., Eds.; CRC Press: Boca Raton, FL, USA, 1997; pp. 271–285.
10. Adamson, D.T.; de Blanc, P.C.; Farhat, S.K.; Newell, C.J. Implications of matrix diffusion on 1, 4-dioxane persistence at contaminated groundwater sites. *Sci. Total Environ.* **2016**, *562*, 98–107. [CrossRef]
11. Ding, X.H.; Feng, S.J. Contaminant back-diffusion from layered aquitards subjected to barrier-controlled source zones. *Water Res.* **2023**, *238*, 120021. [CrossRef]
12. Sale, T.C.; Zimbron, J.A.; Dandy, D.S. Effects of reduced contaminant loading on downgradient water quality in an idealized twolayer granular porous media. *J. Contam. Hydrol.* **2008**, *102*, 72–85. [CrossRef] [PubMed]
13. Parker, B.L.; Chapman, S.W.; Guilbeault, M.A. Plume persistence caused by back diffusion from thin clay layers in a sand aquifer following TCE source-zone hydraulic isolation. *J. Contam. Hydrol.* **2008**, *102*, 86–104. [CrossRef] [PubMed]
14. Carey, G.R.; Chapman, W.S.; Parker, B.L.; McGregor, R. Application of an adapted version of MT3DMS for modeling back-diffusion remediation timeframes. *Remediation* **2015**, *25*, 55–79. [CrossRef]
15. Liu, C.; Ball, W.P. Back diffusion of chlorinated solvent contaminants from a natural aquitard to a remediated aquifer under well controlled filed conditions: Predictions and measurements. *Ground Water* **2002**, *40*, 175–184. [CrossRef]
16. Tatti, F.; Petrangeli Papini, M.; Raboni, M.; Viotti, P. Image analysis procedure for studying back-diffusion phenomena from low-permeability layers in laboratory tests. *Sci. Rep.* **2016**, *6*, 30400. [CrossRef] [PubMed]
17. Wanner, P.; Hunkeler, D. Carbon and chlorine isotopologue fractionation of chlorinated hydrocarbons during diffusion in water and low permeability sediments. *Geochim. Cosmochim. Acta* **2015**, *157*, 198–212. [CrossRef]
18. Yang, M.; Annable, M.D.; Jawitz, J.W. Back diffusion from thin low permeability zones. *Environ. Sci. Technol.* **2015**, *49*, 415–422. [CrossRef]
19. You, X.; Liu, S.; Dai, C.; Guo, Y.; Zhong, G.; Duan, Y. Contaminant occurrence and migration between high-and low-permeability zones in groundwater systems: A review. *Sci. Total Environ.* **2020**, *743*, 140703. [CrossRef]
20. Chapman, S.W.; Parker, B.L.; Sale, T.C.; Doner, L.A. Testing high resolution numerical models for analysis of contaminant storage and release from low permeability zones. *J. Contam. Hydrol.* **2012**, *136–137*, 106–116. [CrossRef]
21. Seyedabbasi, M.A.; Newell, C.J.; Adamson, D.T.; Sale, T.C. Relative contribution of DNAPL dissolution and matrix diffusion to the long-term persistence of chlorinated solvent source zones. *J. Contam. Hydrol.* **2012**, *134–135*, 69–81. [CrossRef]
22. Wanner, P.; Parker, B.L.; Hunkeler, D. Assessing the effect of chlorinated hydrocarbon degradation in aquitards on plume persistence due to back-diffusion. *Sci. Total Environ.* **2018**, *633*, 1602–1612. [CrossRef] [PubMed]

23. Yang, M.; Annable, M.D.; Jawitz, J.W. Forward and back diffusion through argillaceous formations. *Water Resour. Res.* **2017**, *53*, 4514–4523. [CrossRef]
24. Mohrlok, U.; Kirubaharan, C.S.; Eldho, T.I. Transport characteristic in a 3D groundwater circulation flow field by experimental and numerical investigation. Practice periodical of hazardous, toxic, and radioactive. *Waste Manag.* **2010**, *14*, 185–194.
25. Yang, M.; Annable, M.D.; Jawitz, J.W. Light reflection visualization to determinate solute diffusion into clays. *J. Contam. Hydrol.* **2014**, *161*, 1–9. [CrossRef] [PubMed]
26. Cenedese, A.; Viotti, P. Lagrangian analysis of nonreactive pollutant dispersion in porous media by means of the particle image velocimetry technique. *Water Resour. Res.* **1996**, *32*, 2329–2343. [CrossRef]
27. Citarella, D.; Cupola, F.; Tanda, M.G.; Zanini, A. Evaluation of dispersivity coefficients by means of a laboratory image analysis. *J. Contam. Hydrol.* **2015**, *172*, 10–23. [CrossRef] [PubMed]
28. Cupola, F.; Tanda, M.G.; Zanini, A. Laboratory estimation of dispersivity coefficients. *Procedia Environ. Sci.* **2015**, *25*, 74–81. [CrossRef]
29. Huang, W.E.; Smith, C.C.; Lerner, D.N.; Thornton, S.F.; Oram, A. Physical modelling of solute transport in porous media: Evaluation of an imaging technique using UV excited fluorescent dye. *Water Res.* **2002**, *36*, 1843–1853. [CrossRef]
30. Luciano, A.; Viotti, P.; Papini, M.P. Laboratory investigation of DNAPL migration in porous media. *J. Hazard. Mater.* **2010**, *176*, 1006–1017. [CrossRef]
31. Zinn, B.; Meigs, L.C.; Harvey, C.F.; Haggerty, R.; Peplinski, W.J.; Freiherr Von Schwerin, C. Experimental visualization of solute transport and mass transfer processes in two-dimensional conductivity fieldswith connected regions of high conductivity. *Environ. Sci. Technol.* **2004**, *38*, 3916–3926. [CrossRef]
32. Chowdhury, A.I.A.; Gerhard, J.I.; Reynolds, D.; Sleep, B.E.; O'Carroll, D.M. Electrokinetic-enhanced permanganate delivery and remediation of contaminated low-permeability porous media. *Water Res.* **2017**, *113*, 215–222. [CrossRef]
33. Gill, R.T.; Thornton, S.F.; Harbottle, M.J.; Smith, J.W.N. Electrokinetic migration of nitrate through heterogeneous granular porous media. *Groundw. Monit. Rem.* **2015**, *35*, 46–56. [CrossRef]
34. Clifton, L.M.; Dahlen, P.R.; Johnson, P.C. Effect of dissolved oxygen manipulation on diffusive emissions from NAPL-impacted low-permeability soil layers. *Environ. Sci. Technol.* **2014**, *48*, 5127–5135. [CrossRef] [PubMed]
35. Cavanagh, B.A.; Johnson, P.C.; Daniels, E.J. Reduction of diffusive contaminant emissions from a dissolved source in a lower permeability layer by sodium persulfate treatment. *Environ. Sci. Technol.* **2014**, *48*, 14582–14589. [CrossRef] [PubMed]
36. Chokejaroenrat, C.; Comfortc, S.; Sakulthaew, C.; Dvoraka, B. Improving the treatment of non-aqueous phase TCE in low-permeability zones with permanganate. *J. Hazard. Mater.* **2014**, *268*, 177–184. [CrossRef] [PubMed]
37. Tatti, F.; Papini, M.P.; Torretta, V.; Mancini, G.; Boni, M.R.; Viotti, P. Experimental and numerical evaluation of Groundwater Circulation Wells as a remediation technology for persistent, low permeability contaminant source zones. *J. Contam. Hydrol.* **2019**, *222*, 89–100. [CrossRef]
38. Borden, R.C.; Cha, K.Y. Evaluating the impact of back-diffusion on groundwater cleanup time. *J. Contam. Hydrol.* **2021**, *243*, 103889. [CrossRef]
39. Kurawasa, T.; Takanashi, Y.; Suzuki, M.; Inoue, K. Laboratory Flushing Tests of Dissolved Contaminants in Heterogeneous Porous Media with Low-Conductivity Zones. *Wat. Air Soil Poll.* **2023**, *234*, 240. [CrossRef]
40. Tatti, F.; Petrangeli Papini, M.; Sappa, G.; Raboni, M.; Arjmand, F.; Viotti, P. Contaminant back-diffusion from low-permeability layers as affected by groundwater velocity: A laboratory investigation by box model and image analysis. *Sci. Total Environ.* **2018**, *622–623*, 164–171. [CrossRef]